

---

# The family of toxin-related ecto-ADP-ribosyltransferases in humans and the mouse

---

GUSTAVO GLOWACKI,<sup>1</sup> RICKMER BRAREN,<sup>1</sup> KATHRIN FIRNER,<sup>1</sup> MARION NISSEN,<sup>1</sup> MAREN KÜHL,<sup>1</sup> PEDRO RECHE,<sup>2</sup> FERNANDO BAZAN,<sup>2</sup> MARINA CETKOVIC-CVRLJE,<sup>3</sup> EDWARD LEITER,<sup>3</sup> FRIEDRICH HAAG,<sup>1</sup> AND FRIEDRICH KOCH-NOLTE<sup>1</sup>

<sup>1</sup>Institute of Immunology, University Hospital, D-20246 Hamburg, Germany

<sup>2</sup>The DNAX Research Institute for Molecular Biology, Palo Alto, California 94304, USA

<sup>3</sup>The Jackson Laboratory, Bar Harbor, Maine 04609, USA

(RECEIVED January 4, 2002; FINAL REVISION April 10, 2002; ACCEPTED April 10, 2002)

## Abstract

ADP-ribosyltransferases including toxins secreted by *Vibrio cholera*, *Pseudomonas aeruginosa*, and other pathogenic bacteria inactivate the function of human target proteins by attaching ADP-ribose onto a critical amino acid residue. Cross-species polymerase chain reaction (PCR) and database mining identified the orthologs of these ADP-ribosylating toxins in humans and the mouse. The human genome contains four functional toxin-related ADP-ribosyltransferase genes (*ARTs*) and two related intron-containing pseudo-genes; the mouse has six functional orthologs. The human and mouse *ART* genes map to chromosomal regions with conserved linkage synteny. The individual *ART* genes reveal highly restricted expression patterns, which are largely conserved in humans and the mouse. We confirmed the predicted extracellular location of the *ART* proteins by expressing recombinant *ARTs* in insect cells. Two human and four mouse *ARTs* contain the active site motif (R-S-EXE) typical of arginine-specific ADP-ribosyltransferases and exhibit the predicted enzyme activities. Two other human *ARTs* and their murine orthologues deviate in the active site motif and lack detectable enzyme activity. Conceivably, these *ARTs* may have acquired a new specificity or function. The position-sensitive iterative database search program PSI-BLAST connected the mammalian *ARTs* with most known bacterial ADP-ribosylating toxins. In contrast, no related open reading frames occur in the four completed genomes of lower eucaryotes (yeast, worm, fly, and mustard weed). Interestingly, these organisms also lack genes for ADP-ribosylhydrolases, the enzymes that reverse protein ADP-ribosylation. This suggests that the two enzyme families that catalyze reversible mono-ADP-ribosylation either were lost from the genomes of these nonchordata eucaryotes or were subject to horizontal gene transfer between kingdoms.

**Keywords:** ADP-ribosylation; recombinant proteins; PSI-BLAST; orthologous genes; paralogous gene; cross-species PCR; database searches

---

Reprint requests to: Friedrich Koch-Nolte, Institute for Immunology, University Hospital, Martinistr. 52, D-20246 Hamburg, Germany, e-mail: nolte@uke.uni-hamburg.de; fax: 49-40-42803-4243.

**Abbreviations:** ARH, ADP-ribosylhydrolase; GAPD, glyceraldehyde-3-phosphate dehydrogenase; GPI, glycosylphosphatidylinositol; HPRT, hypoxanthine phosphoribosyltransferase; mART, mono(ADP-ribosyl)transferase; NAD<sup>+</sup>, nicotine adenine dinucleotide; PBS, phosphate-buffered saline; pART, poly(ADP-ribosyl)transferase; PCR, polymerase chain reaction; RACE, rapid amplification of cDNA ends; RT, reverse transcription; RFLV, restriction fragment length variant; SDS-PAGE, sodium dodecyl sulfate polyacrylamide gel electrophoresis; utr, untranslated region.

Article and publication are at <http://www.proteinscience.org/cgi/doi/10.1110/ps.0200602>.

The purpose of this study was to identify all recognizable human and mouse members of the family of toxin-related mono-ADP-ribosyltransferases; to clone, sequence, and chromosomally map their genes and cDNAs; to express the gene products as recombinant proteins and assay their enzyme activities; and to assess structural and sequence similarities between bacterial and mammalian ADP-ribosyltransferases.

ADP-ribosylation is an enzyme-catalyzed post-translational protein modification in which the ADP-ribose moiety is transferred from NAD<sup>+</sup> to a specific amino acid in a

target protein while the nicotinamide moiety is released (Althaus et al. 1985; Jacobson and Jacobson 1989; Aktories 1991; Haag and Koch-Nolte 1997; Rappuoli and Montecucco 1997; Smith 2001). This stereospecific reaction is catalyzed by mono- and poly-ADP-ribosyltransferases (mARTs and pARTs). mARTs catalyze the transfer of a single ADP-ribose moiety onto a specific amino acid side chain of a target protein; pARTs (also designated poly-ADP-ribose-polymerases or PARPs), additionally can catalyze the elongation and branching of ADP-ribose units on ADP-ribosylated targets. In the absence of target proteins, some ARTs also exhibit NAD-glycohydrolase (NADase) activity. The mART subfamily includes many well-known bacterial toxins as well as a number of mammalian and avian ecto-enzymes. Members of the pART subfamily have been identified in a broad spectrum of eucaryotes, including man, *Drosophila*, *Arabidopsis*, but not in yeast or prokaryotes.

Most known mARTs transfer ADP-ribose onto arginine residues. Arginine-specific ARTs include cholera toxin and *Escherichia coli* heat-labile enterotoxin, which target the alpha-subunit of heterotrimeric G-proteins; C2 toxin of *Clostridium botulinum*, VIP2 of *Bacillus cereus*, and SpvB of *Salmonella entericae*, all of which target actin; ALT of T4-bacteriophage, which targets *E. coli* RNA-polymerase; DRAT of *Rhodospirillum rubrum*, which targets dinitrogenase reductase; ExoS of *Pseudomonas aeruginosa*, which targets ras; and mouse ART1 and ART2, which target integrins and other cell surface proteins (Aktories 1991; Ludden 1994; Haag and Koch-Nolte 1997; Rappuoli and Montecucco 1997; Okazaki and Moss 1998; Han et al. 1999; Otto et al. 2000). Additionally, mARTs have been identified, which specifically target the side chains of other amino acid residues, including diphthamide in elongation factor 2 (diphtheria toxin and pseudomonas exotoxin A); cysteine in inhibitory G-proteins (pertussis toxin); asparagine in rho and related small GTP binding proteins (C3 exoenzymes of *Clostridium botulinum* and *Staphylococcus aureus*) (Aktories 1991; Wilson and Collier 1992; Barbieri 2000; Wilde et al. 2001). In contrast, pARTs (e.g., PARP, tankyrase) target glutamic acid in histones, telomerase binding protein, and others (Burkle 2001; Smith 2001).

Like phosphorylation, ADP-ribosylation is a reversible post-translational modification that can be used as a mechanism to regulate endogenous protein functions. A reversible ADP-ribosylation cycle was first corroborated in the photosynthetic bacterium *Rhodospirillum rubrum*, in which nitrogen fixation is regulated by an mART-mediated ADP-ribosylation of the key enzyme dinitrogenase reductase (Ludden 1994). An ADP-ribosylhydrolase (ARH) reverses ADP-ribosylation of dinitrogenase reductase. (This ARH is designated dinitrogenase reductase ADP-ribosylarginine glycohydrolase or DRAG). A homolog of this enzyme, des-

ignated ADP-ribosylarginine hydrolase (ARH), has been identified in humans and mice (Moss et al. 1992).

ARTs show remarkable plasticity in amino acid sequences, a feature that hampers the in silico identification of distant gene family members (Domenighini and Rappuoli 1996; Koch-Nolte et al. 1996a; Bazan and Koch-Nolte 1997; Okazaki and Moss 1998). The crystal structures of eight bacterial toxins and of chicken PARP uncovered common features of the NAD-binding pocket: a unique topology of six conserved  $\beta$ -strands and an  $\alpha$ -helix form the upper and lower jaws of a Pacman-like active site crevice (Choe et al. 1992; Ruf et al. 1996; Han et al. 1999, 2001). Only a single amino acid residue, the catalytic glutamic acid residue in the fifth  $\beta$ -strand, is strictly conserved in all structures (Carroll and Collier 1984). Two other conserved residues in the first and second  $\beta$ -strand (arginine and serine in most mARTs, histidine and tyrosine in the two diphthamide-specific mARTs, and in all known pARTs have been used to divide the ART family into two subgroups, i.e., the R-S-E motif group and the H-Y-E motif group) (Domenighini and Rappuoli 1996; Koch-Nolte et al. 1996a; Bazan and Koch-Nolte 1997). A second glutamic acid, two residues upstream of the catalytic E in the loop connecting the fourth and fifth  $\beta$ -strand, is found in all arginine-specific ARTs, by far the largest subfamily of known ARTs (R-S-EXE).

Recent improvements in database search tools, in particular the development of the iterative, position-sensitive PSI-BLAST program, have made it possible to identify distant protein family members even when they share only very limited amino acid sequence identities (Altschul and Koonin 1998). PSI-BLAST generates a search matrix on the basis of a multiple sequence alignment in which conserved residues are given a higher weight than nonconserved residues. Here, we describe the use of this tool to provide evidence that mammalian mARTs indeed are related to ADP-ribosylating toxins. Moreover, the results uncover remarkable "holes" in the phylogeny of mARTs in the completed genomes of yeast, worm, fly, and mustard weed. Remarkably, this distribution pattern is mirrored by similar "holes" in the phylogeny of the ARH family.

## Results

### *Identification, cloning, and sequencing of human and mouse ART/Art genes*

To identify and clone the members of the gene family of toxin-related mARTs from the human and the mouse, we used a combination of strategies. First, we derived degenerate PCR primers corresponding to conserved regions of known mammalian ART1–ART5 and used these for cross-species "Zoo"-PCR analyses. A representative result is shown in Figure 1. PCR products of the expected size were

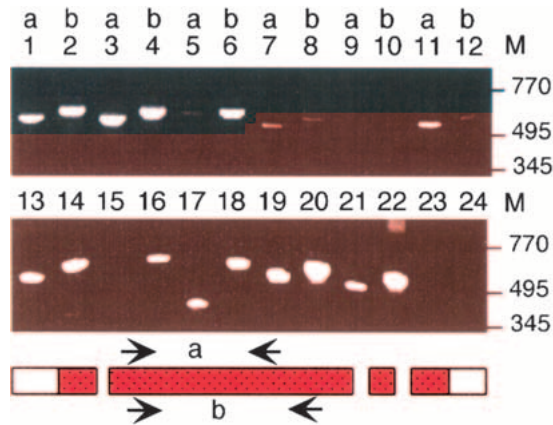


**Fig. 1.** Cross-species "Zoo"-PCR analyses of *ART5*. Genomic DNAs were subjected to PCR-amplification with two pairs of *ART5*-specific primers (a and b) ending in codons for conserved amino acids. Reaction products were size fractionated by agarose gel electrophoresis and visualized by staining with ethidium bromide. Genomic DNAs were from: rhesus monkey: lanes 1–2, macaque monkey: lanes 3–4, pig: lanes 5–6, rat: lanes 7–8, control ( $H_2O$ ): lanes 9–10, mouse: lanes 11–12, human: lanes 13–14, tree shrew: lanes 15–16, house shrew: lanes 17–18, cow: lanes 19–20, sheep: lanes 21–22, chicken: lanes 23–24. M = size of marker fragments in base pairs.

generated from genomic DNAs of most organisms analyzed. These were then subcloned and sequenced. The results revealed that in the vast majority of cases, the PCR products derived from the respective *ART* ortholog. Thereby, we obtained fragments of hitherto unknown murine *Art3* and *Art4* starting from the known sequences of human *ART3* and *ART4* (Koch-Nolte et al. 1997). Similarly, starting from the known sequence of mouse *Art5*, we obtained a fragment of the hitherto unknown human *ART5* gene (Okazaki et al. 1996; Glowacki et al. 2001). Moreover,

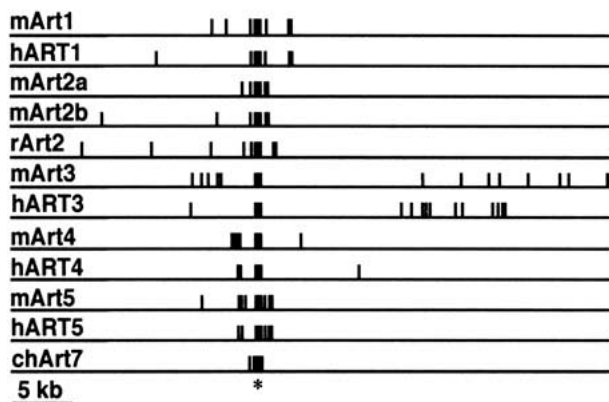


**Fig. 2.** Schematic diagram of *ART* gene exon/intron structures. Exons and flanking introns were sequenced from respective P1 and PAC genomic DNA clones. Exons are depicted as closed boxes, introns and flanking regions as lines. Genes were aligned with respect to the major exon encoding the catalytic domain (\*). The sizes of exons and introns are shown in Figure 4.

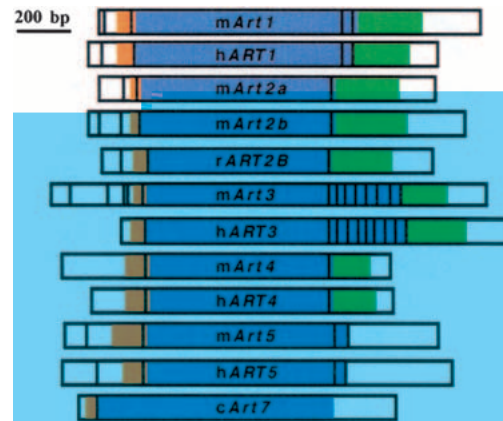


**Fig. 3.** Schematic diagrams of the *ART* cDNA exon compositions. The major splice variant is depicted for each *ART* gene transcript. Noncoding 5' and 3' untranslated regions are white, coding regions are color coded: leader peptide: orange, native peptide: blue, GPI-anchor signal: green.

we thus obtained respective *ART* sequences from several other mammalian species. Occasionally, cloned Zoo-PCR products contained, in addition to the *ART*-ortholog, a fragment derived from an evident *ART*-paralog. These always corresponded to one of the other known *ARTs* (*ART1*–*5*). Full-length cDNA and genomic clones were then obtained for all known human and mouse *ART* genes by classic cloning techniques (Figs. 2, 3).

To determine whether the human or other mammalian genomes contain additional *ART* gene family members, we next used the deduced full-length human and mouse *ART1*–*ART5* amino acid sequences as input for database searches (Table 1). The tBLASTn program was used to search nucleotide databases, and PSI-BLAST to search protein da-

**Table 1.** Chromosomal localization and dbEST representation of the human and mouse *ART* and *ARH* gene families

	Human			Mouse		
	gb	ESTs	Band	gb	ESTs	cM
<i>ART1</i>	S74683	1	11p15	X95825	49	7.49
<i>ART2A</i>	X65060	0	11q13	X52991	3	7.48
<i>ART2B</i>	na	0	11q13	X87612	1	7.48
<i>ART3</i>	X95827	40	4q13.1–q13.3	AJ311769	82	5.51
<i>ART4</i>	X95826	12	12p12.2–p13.1	Y08300	3	6.70
<i>ART5</i>	Y16836	6	11p15	Y08028	12	7.49
<i>ARH1</i>	L13291	1	3q13.31–33	L13290	145	na
<i>ARH2</i>	A1333260	23	13q31	A1503324	24	na
<i>ARH3</i>	AJ313333	135	1p34.1–35.3	AW209835	50	na
<i>GAPD</i>	M33197	7541	12p13	M32599	1854	6
<i>HPRT</i>	M31642	120	Xq26.1	J00432	276	X

The number of matching expressed sequence tags (ESTs) in the public database (release June 2001) is given for each gene. Chromosomal localizations are shown as cytogenetic bands for the human and as distances from the centromere in cM for the mouse.

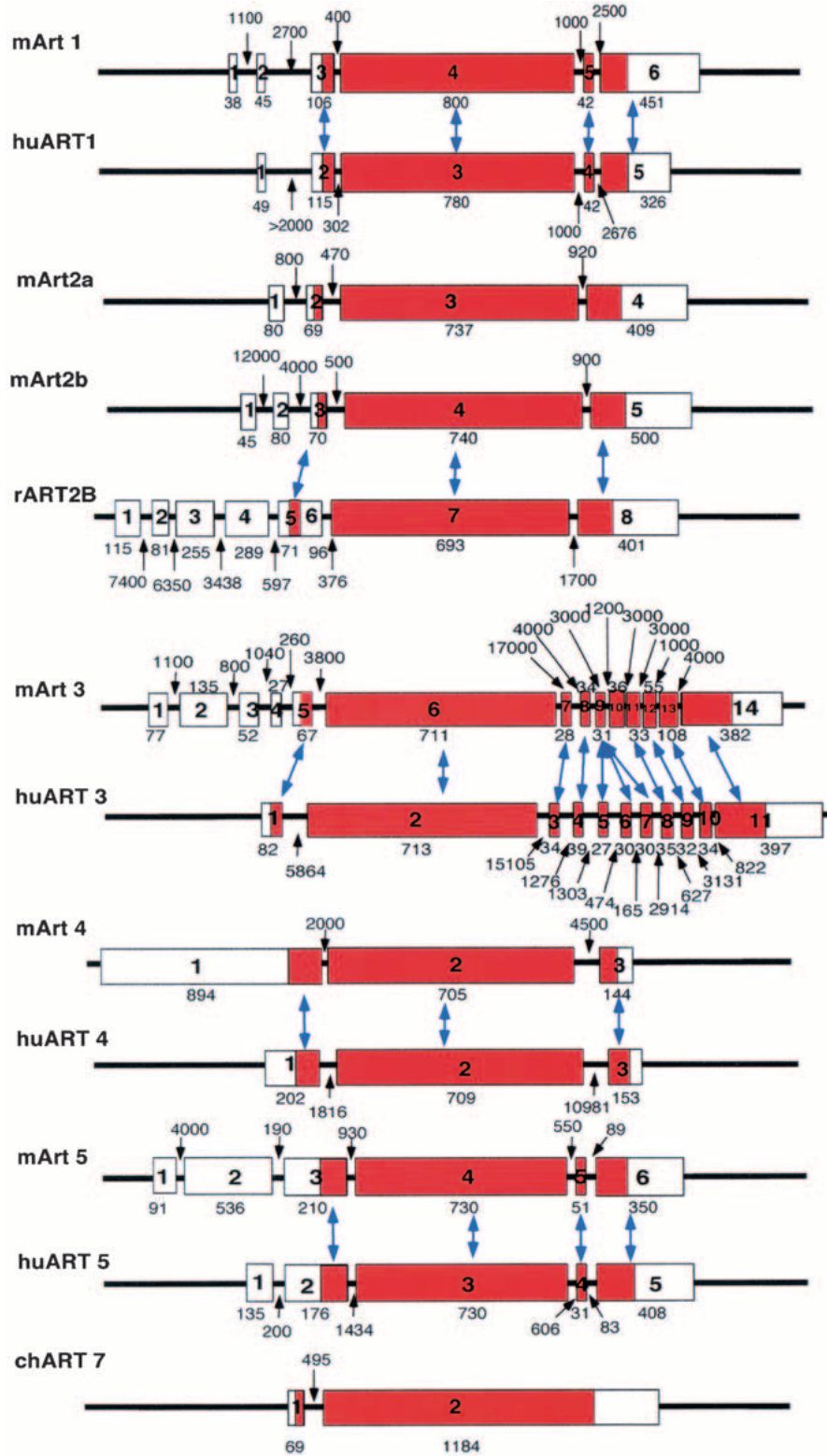


**Fig. 4.** Exon-intron structures of human and mouse *ART* genes. Exons are depicted as boxes, introns as lines. Numbers indicate lengths of exons and introns in base pairs. Corresponding exons in *ART* orthologs are connected by arrows. Note that a small exon in the 3' coding region of human *ART3* is triplicated with respect to its mouse *Art3*.



**Fig. 5** Amino acid sequence alignments of orthologs ARTs. Alignments of the deduced amino acid sequences of each pair of ART-orthologs are shown with the human sequence on top and mouse sequence on bottom. Conserved residues are shown in the middle of each alignment. Predicted secondary structure units lining the six conserved  $\beta$  strands of the active site crevice are marked below the alignment. Different colors are used for amino acids encoded by different exons. The four cysteine residues common to all ARTs are highlighted in yellow, additional ART-specific pairs of cysteine are marked by asterisks. Potential asparagine-linked glycosylation sites are highlighted in blue. Residues corresponding to the R-S-EXE motif of arginine-specific ARTs are highlighted in green. Three premature stop codons of human ART2AP are marked in red.

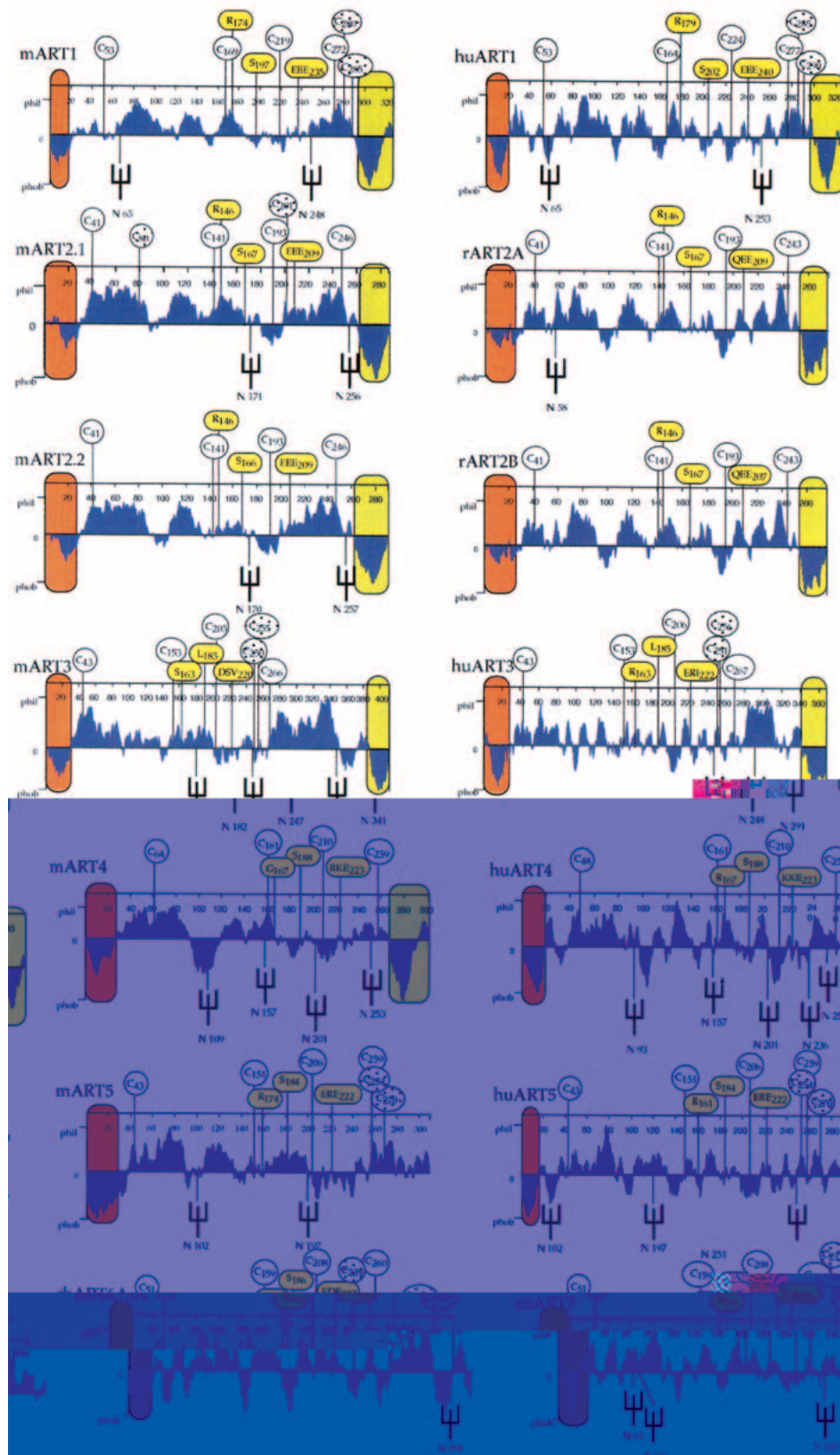


**Fig. 6.** Hydropathy profiles of human and mouse ART proteins. Hydropathy profiles were calculated with a window setting of 19 amino acid residues. Putative hydrophobic amino- and carboxy-terminal signal peptides are colored orange and green, respectively. Positions of potential asparagine-linked oligosaccharide side chains are marked by forks. The four cysteine residues conserved in all mammalian ARTs are marked by circles with numbers indicating their respective positions from the amino terminus. Additional cysteine residues found only in individual ARTs are marked by shaded circles. Residues corresponding to the R-S-EXE motif of arginine specific mARTs are marked by yellow circles.

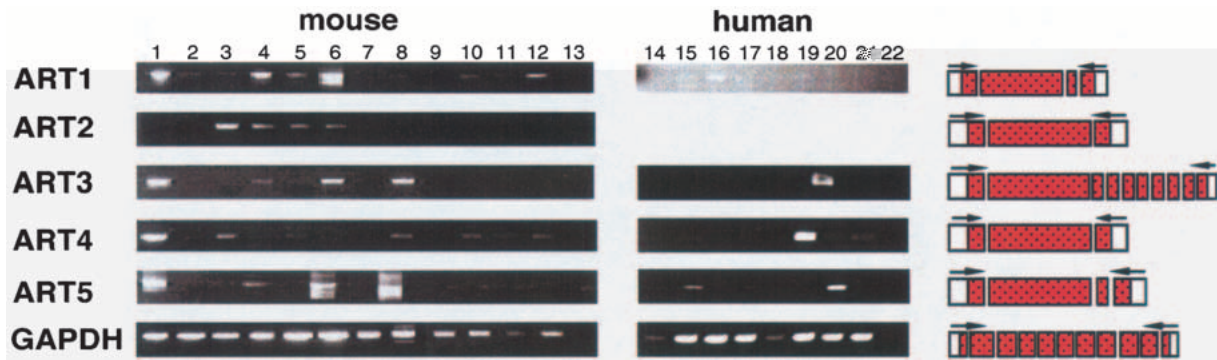


**Fig. 7.** Reverse transcription PCR analyses of *ART* gene expression. Panels of mouse and human cDNAs were subjected to reverse transcription PCR analyses using primers from separate exons as illustrated schematically. Products after 31 cycles were size fractionated by agarose gel electrophoresis and visualized by ethidium bromide staining. cDNAs were from: heart: lane 1, brain: lane 2, spleen: lane 3, lung: lane 4, liver: lane 5, skeletal muscle: lane 6, kidney: lane 7, testis: lane 8, 7-day embryo: lane 9, 11-day embryo: lane 10, 15-day embryo: lane 11, 17-day embryo: lane 12, control (H<sub>2</sub>O): lane 13, colon: lane 14, ovary: lane 15, peripheral blood lymphocytes: lane 16, prostate: lane 17, small intestine: lane 18, spleen: lane 19, testis: lane 20, thymus: lane 21, and control (H<sub>2</sub>O): lane 22.

tabases. tBLASTn can detect significant amino acid sequence homologies (>25% sequence identity) encoded in nucleotide sequences. PSI-BLAST can detect much more distantly related sequences (<5% amino acid sequence identity), but is restricted to the database of protein sequences (Altschul and Koonin 1998). Previous studies (Braren et al. 1997; Koch-Nolte et al. 1997) have demonstrated that tBLASTn can successfully detect paralogous mammalian *ART*-sequences (e.g., *ART3*, 4, and 5 using *ART1* and *ART2* as input). This is facilitated by the fact that a single large exon typically encodes most of the native protein of mammalian *ARTs* (Fig. 3).

tBLASTn searches of the recently completed human genome sequence (Lander et al. 2001) revealed only a single hitherto unknown pseudogene (designated *ART2BP*) in addition to the already identified *ART2* pseudogene (Haag et al. 1994) and four functional human *ART* gene family members (*ART1*, *ART3*, *ART4*, and *ART5*) (Okazaki et al. 1994; Koch-Nolte et al. 1997) (Table 1). The mouse has functional orthologs for each of these genes (designated *Art1*, *Art2a*, *Art2b*, *Art3*, *Art4*, and *Art5*). tBLASTn searches of the EST database identified one or more EST derived from each of the functional murine and human *ART* genes, but did not reveal any other related paralogue (Table 1). Similarly, PSI-BLAST searches did not uncover any other mammalian *ART*-paralogs in the protein database, but did connect the mammalian *ARTs* with ADP-ribosylating bacterial toxins (see below).

#### *Chromosomal localization and exon/intron structures of mouse and human Art/ART genes*

We determined the chromosomal localization of human *ART* genes by PCR screening of human–mouse somatic cell

hybrids and confirmed the assignments by sequence similarity searches of the completed human genome sequence (Lander et al. 2001). To map the mouse *Art* genes we first identified an informative allelic polymorphism for each *Art* gene and then determined its distribution in a panel of genomic DNAs from a backcross of (*C57BL/6J* × *Mus spretus*) × *Mus spretus* (Table 1). All *ART* orthologs mapped to regions of conserved linkage synteny. Interestingly, *ART1* and *ART5* are arranged in a “head-to-head” orientation in close proximity in both the mouse (Glowacki et al. 2001) and humans.

The exon/intron structures of all human and mouse *ART* genes were determined by comparative sequencing of full-length cDNA and genomic DNA clones (Fig. 2). In each case, a single long exon encodes most of the native protein, whereas separate exons encode the N- and C-terminal signal peptides (Fig. 4). *ART2* and *ART4* do not contain any additional coding exons. *ART1* and *ART5* contain one additional small exon encoding the C-terminal end of the native protein. *ART3* contains several small exons in this region. The 5′ untranslated region is split into several distinct exons in most *ART* genes (Fig. 4). These results confirm and markedly extend previous findings on the gene structures of mouse *Art1* (Braren et al. 1998), rat *ART2* (Haag et al. 1996), and mouse *Art5* (Glowacki et al. 2001).

#### *Common and distinctive features of the deduced ART amino acid sequences*

All *ARTs* contain hydrophobic N-terminal peptides that exhibit high signal sequence probabilities (Figs. 5, 6). The predicted extracellular localization was confirmed by expression cloning in insect cells (see below). All human and mouse *ARTs* except for *ART5* end in a second prominent

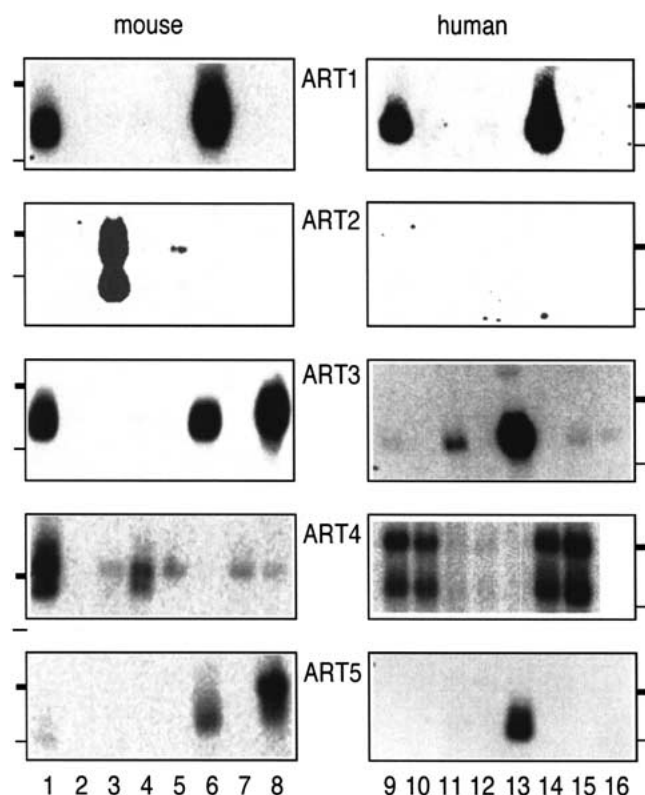


**Fig. 8** Northern blot analyses of human and mouse *ART* gene expression. Northern blots with mouse and human RNAs were hybridized with radio-labeled *ART*-specific probes, and bound activity was visualized by autoradiography. Thick and thin bars indicate the migration positions of 2.4kb and 1.35kb marker fragments, respectively. Mouse RNAs were from heart: lane 1; brain: 2; spleen: 3; lung: 4; liver: 5; skeletal muscle: 6; kidney: 7; and testis: 8. Human RNAs for *ART1* and *ART2* were from heart: lane 9; brain: 10; placenta: 11; lung: 12; liver: 13; skeletal muscle: 14; kidney: 15; and pancreas: 16; for *ART3* and *ART5*, pancreas: lane 9; adrenal medulla: 10; thyroid: 11; adrenal cortex: 12; testis: 13; thymus: 14; small intestine: 15; and stomach: 16; and for *ART4*, spleen: lane 9; lymph node: 10; thymus: 11; appendix: 12; peripheral blood leukocytes: 13; bone marrow: 14; and fetal liver: 15.

stretch of hydrophobic amino acids, a characteristic feature of GPI-anchored membrane proteins. Four cysteine residues are strictly conserved in all mammalian ART proteins. These are also found in the three known avian ecto-ARTs. Structure-based alignments of mammalian ARTs and bacterial ARTs of known structure indicate that the second and third cysteine residues lie in close proximity, and therefore, probably form a disulfide bond. Human and mouse *ART1*, *ART3*, and *ART5* each contain an extra pair of cysteine residues near the C-terminal end. The positions of these residues are conserved in the respective species orthologs but not among paralogues. Human and mouse *ART1*, *ART5*, and mouse *ART2.1*, *ART2.2* contain residues corresponding to the R-S-EXE motif of arginine specific mARTs. *ART3* and *ART4* of both the human and the mouse show nonconservative amino acid deviations in this motif (Figs. 5, 6).

#### Tissue-specific expression patterns of *ART* genes

To determine whether human and mouse *ART* genes are expressed ubiquitously or in a tissue-restricted manner, we performed semiquantitative reverse transcription PCR (RT-PCR) (Fig. 7) and serial Northern blot analyses (Fig. 8). The results reveal restricted expression patterns for the individual *ART* genes. *ART1* is most prominently expressed in skeletal muscle, *ART2* in T cells, *ART3* and *ART5* in testis. *ART4* shows a broader pattern of expression with prominent signals in heart, lung, liver, and spleen. Tissue specificity is largely conserved in the human and mouse.

#### Recombinant expression and enzymatic analysis of epitope-tagged soluble ARTs

We designed insect cell expression constructs to test the function of the putative N-terminal signal sequences. In case of *ART1*–*ART4*, we deleted the GPI anchor signal sequence to obtain soluble proteins. Engineered C-terminal epitope tags allowed their detection and purification. Indeed, the ART proteins were efficiently produced and secreted by transfected insect cells (Fig. 9A). Using established enzyme assays (Haag et al. 1995; Koch-Nolte et al. 1996b; Braren et al. 1998) we demonstrated potent arginine-specific ADP-ribosylation activity for human and mouse *ART1*, mouse *ART2.1* and *ART2.2*, and human *ART5* (Fig. 9B). Mouse *ART5* resembles rat *ART2* (Haag et al. 1995) in showing

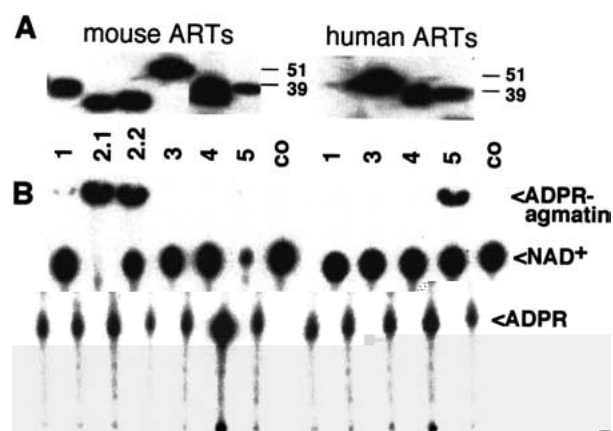


**Fig. 9** Comparative enzyme assays of purified epitope-tagged ARTs. ARTs were immunoprecipitated from the supernatants of respective baculovirus-infected insect cells with immobilized anti-FLAG monoclonal antibody M2. Purified ARTs were incubated with  $^{32}\text{P}$ -NAD $^{+}$  for 60 min at 37°C in the presence of 2 mM agmatine (an arginine analog). Proteins were analyzed by SDS-PAGE and Western blot analyses using the anti-FLAG antibody (A). Note that human *ART1* was not produced efficiently in this system (A, lane 7). Enzyme reaction products were analyzed by thin-layer chromatography followed by autoradiography (B). Co: control precipitates from mock infected cells.

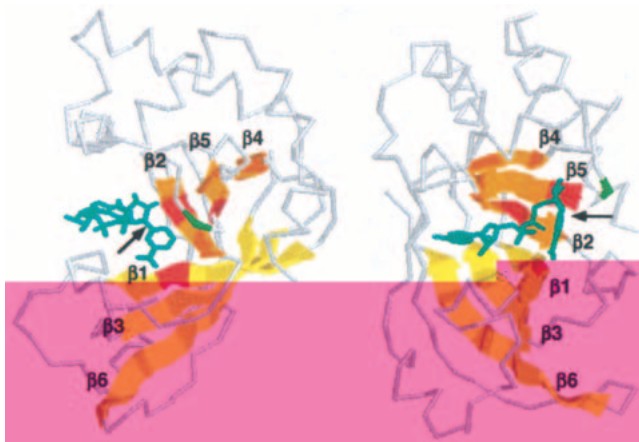


**Fig. 10.** Matches detected by PSI-BLAST cluster in regions corresponding to the active site crevice of VIP2. Regions shown in the multiple sequence alignment (Fig. 11) are projected onto the backbone of *Bacillus cereus* VIP2 (Han et al. 1999) with bound NAD (cyan). The two images generated by rasmac using pdb file 1QS2 are rotated by 90° to provide side (*left*) and front (*right*) views of the active site crevice. The arrow points to the cleaved bond in NAD. The six conserved  $\beta$ -strands of the lower and upper jaws of the active site crevice are depicted as cartoons and are colored yellow ( $\beta 4$ ,  $\beta 5$ ,  $\beta 2$ ) and orange ( $\beta 1$ ,  $\beta 3$ ,  $\beta 6$ ), respectively. The three residues of the R-S-E motif are in red, the upstream glutamic acid of arginine-specific mARTs is in green.

potent NAD-glycohydrolase activity. Neither mouse nor human ART3 and ART4 showed any detectable enzyme activities in these assays.

*The deduced ART amino acid sequences exhibit conserved structural motifs and amino acid sequence similarities with ADP-ribosylating toxins*

To assess possible structural and sequence similarities between mammalian and bacterial mARTs we used secondary structure prediction and position sensitive database search programs (PHDsec and PSI-BLAST) (Rost and Sander 1993; Altschul and Koonin 1998). The N-terminal portion of mammalian ARTs is predicted to be mainly helical; the C terminal region is dominated by  $\beta$ -sheets. This pattern of secondary structure units is very similar to those of the catalytic domains in the recently crystallized ADP-ribosylating bacterial toxins VIP2 of *Bacillus cereus* and C3 of *Clostridium botulinum* (Han et al. 1999, 2001) (Fig. 10). Moreover, PSI-BLAST connected mammalian mARTs with most known bacterial mARTs (Table 2). The overall sequence identities between vertebrate and bacterial mARTs are <10%, that is, deep in the “twilight zone” of traditional search programs. Significantly, the matches detected by PSI-BLAST cluster in regions corresponding to the active site crevice in VIP2, C3, and other bacterial toxins of known 3D structures (Figs. 10, 11).

*PSI-BLAST analyses reveal similar “holes” in the phylogenies of ARTs and ARHs*

Remarkably, none of the four other recently elucidated eucaryotic genomes (those of a yeast, a worm, a fly, and a plant) contains any predicted open reading frame as or more closely related to the mammalian ARTs as the bacterial toxins (Table 3). We wondered whether comparable “holes” in phylogeny also occurred in the ARH family, that is, the enzymes reversing ADP-ribosylation. Indeed, bacterial and human ARHs were connected by PSI-BLAST, whereas no significant matches were detected in the other four com-

**Table 2.** Tiling paths of PSI-BLAST searches with mARTs and ARHs

i	*ART1/H.s.	i	VIP2/B.c.	i	*ARH3/H.s.	
1	ART2/M.m.	1	C2/C.b.	1	*ARH1/H.s.	
	*ART3/H.s.		iota/C.p.		*ORF/A.f	
	*ART4/H.s.		C3/C.b.ph		*ORF/M.j.	
	ART5/M.m.		*EDIN/S.a.		*ORF/A.a	
	ART6/G.g		ToxA/C.d.		*ORF/E.c.	
	ART7/G.g		*ORF/B.h.		ORF/S.c.	
2	*exoS/P.a.	2	*C3/S.a.	2	*ORF/M.I.	
	*exoT/P.a.		*exoS/P.a		DRAG/R.r.	
3	C2/C.b.	3	*exoT/P.a.	3	DRAG/A.b.	
4	*SpvB/S.t.P.	4	*SpvB/S.t.P.	4	ORF/Y.e.	
	VIP2/B.c.		*ORF/S.p.		ORF/L.m.	
	*ORF/B.h.		ALT/E.c.ph		*ORF/D.r.	
5	iota/C.p.	5	ORF/V.p.	5	J1/T.c.	
	C3/C.b.		ART7/G.s.		converged	
	*C3/S.a.		*ART1/H.s.			
	*ORF/S.p.		ART2/M.m	i	DRAG/R.r.	
6	*EDIN/S.a.	6	ART5/M.m.	1	DRAG/A.b.	
	ORF/V.p.		ART6/G.g.		*ORF/M.j.	
7	ALT/E.c.ph	7	ART7/G.g.	7	*ORF/A.f	
	ToxA/C.d.		*ART3/H.s.		*ORF/A.a	
8	converged	8	*ORF/Ch.V.	8	*ORF/E.c.	
			*CT/V.c.		ORF/S.c.	
i	*CT/V.c.	i	*LT/E.c.P.	i	*ORF/M.I.	
1	*LT/E.c.P.	1	DRAT/R.r.	1	*ARH1/H.s.	
2	PT/B.p.	2	DRAT/A.b.	2	*ARH3/H.s.	
3	*MTX/B.s.	3	converged	3	ORF/Y.e.	
	pier/P.r.				ORF/L.m.	
	ORF/S.c.		i	modA/E.c.ph.	*ORF/D.r.	
4	*exoS/P.a	4	1	modB/E.c.ph.	J1/T.c.	
	*exoT/P.a.		2	converged	3	converged
5	converged	5	converged	5	converged	
			i	HvnA/V.f.		
i	*ETA/P.a.	i	1	HvnB/V.f.		
1	DT/C.d.ph	1	*ORF/P.a.			
2	converged	2	converged			

PSI-BLAST searches of the nonredundant public database (June 2001) were initiated with the sequences indicated on top. Searches were repeated in successive iterations using a matrix in which conserved residues are given a higher weight. Converged indicates that no more significant matches were detected. A single ortholog is listed for genes that have been cloned from more than one species. Matches are listed with the protein abbreviation (ORF = open reading frame) followed by abbreviations for species designation. Asterisks mark species with completed genome sequences.

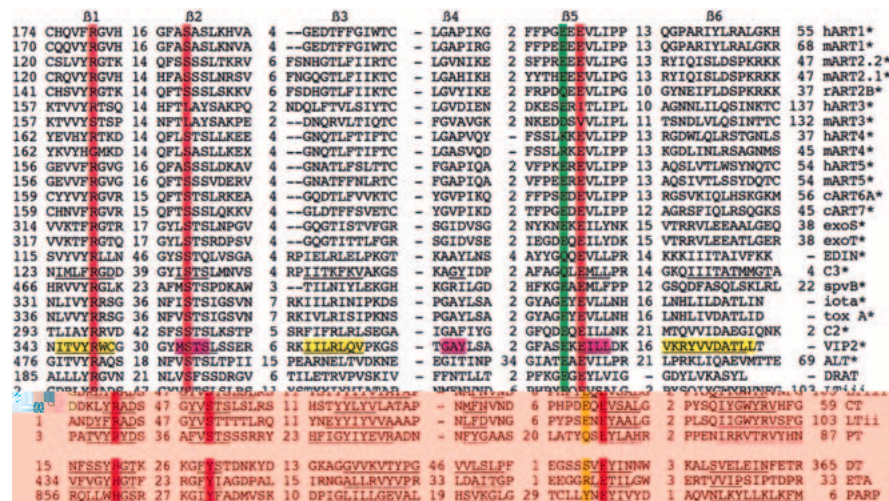


**Fig. 11.** Multiple sequence alignment of the catalytic cores of vertebrate and bacterial mARTs. Multiple amino sequence alignment of the region corresponding to the six conserved  $\beta$ -strands of the active site crevice (see Fig. 10). Nonconserved residues in connecting loops are not shown and are indicated by numbers. Known secondary structure units in the crystallized mARTs are underlined (C3, VIP2, CT, LT, PT, DT, ETA, and PARP). Color coding as in (A). Note that the last  $\beta$  strand in VIP2, C3, and related ARTs (marked by asterisks) has been displaced by a strand in opposite orientation relative to that in LT, PARP, and others (i.e.,  $\beta 5$  and  $\beta 6$  are parallel in VIP2, whereas they are antiparallel in CT).

pleted eucaryotic genomes. Of note, we discovered two hitherto unknown human *ARH* gene family members (designated *ARH2* and *ARH3*), both of which are represented also in dbEST (see Table 1).

## Discussion

In this study, we identified the human and mouse members of the mART and *ARH* gene families (Table 1). The presence of respective orthologs in many mammalian species indicates that these genes were generated by duplication events at or before the mammalian radiation. Most ART genes exhibit a tightly restricted expression pattern and relatively low transcript levels (Figs. 7, 8), possibly reflecting the regulatory function of the ART gene products.

Our enzyme assays with recombinant ARTs confirmed arginine-specific transferase activity for all human and mouse ARTs containing the R-S-EXE motif (Figs. 9, 10). ART3 and ART4 lack this motif, and do not display any detectable arginine-specific enzyme activity, indicating that these family members may have acquired a different target specificity or lost enzyme activity altogether. In this context, it is interesting to point out the following precedents from procaryotic mARTs:

1. Some enzymatically inactive ART domains, for example, the N-terminal domains of C2 and VIP2 toxins, have acquired a new, protein-binding function (Han et al. 1999, 2001). Other examples for the acquisition of novel

functions by inactivated enzyme family members include caspase-related FLIP (Tschopp et al. 1998) and lens crystallins (Piatigorsky 1998).

2. Some mARTs, for example, diphtheria toxin, exhibit a narrow target specificity that would not have been detected with the assays applied here (Wilson and Collier 1992).
3. The enzyme activities of some mARTs, for example, cholera toxin and ExoS, become apparent only after binding to an activator (Rappuoli and Montecucco 1997; Barbieri 2000).

Further studies are required to resolve whether any of these explanations also apply to ART3 and ART4. Note, however, that we did not detect any enzyme activity above background upon adding recombinant ART3 and ART4 proteins to lysates from various cell lines (not shown).

The results of our database searches and structure prediction analyses strongly support an evolutionary relationship of mammalian and bacterial ARTs as well as of mammalian and bacterial ARHs (Fig. 6; Tables 2, 3). Interestingly, both enzyme families evidently are missing in the four fully sequenced genomes and expressed sequence tags of lower eucaryotes. A similar phylogenetic distribution pattern has been observed for 41 human genes, mostly coding for enzymes (Andersson et al. 2001; Lander et al. 2001). This can be explained either by loss of the respective genes from these nonchordata eucaryotes or by horizontal transfer of

**Table 3.** Phylogenetic distribution of ART and ARH genes in completed and unfinished genomes

	Viruses (>500)	Bacteria (33)	Archaea (10)	Eucaria (4)	Vertebr (1)
ARTs in finished genomes	Ch.V./1	P.a./2 V.c./1 S.a./2 B.h./1 B.s./1 S.p./1 E.c.P./1 S.t.P./1	0	0	H.s./5
ARTs in other genomes	E.c.ph/1 C.b.ph/1	B.c./1 C.b./1 C.p./1 V.p./1 R.r./1 A.b./1 S.c./1	0	P.r./1	M.m./6 G.g./3
Unconnected ARTs	C.d.ph/1 E.c.ph/2	P.a./2 V.f./2	0	0	0
ARHs in finished genomes	0	A.a./1 B.h./1 D.r./1 E.c./1	M.j./1 A.f./1	0	H.s./3
ARHs in other genomes	0	R.r./1 A.b./1 Y.e./1 L.m./1 S.c./7	0	T.c./3	M.m./3
pARTs	Ci.V./1	0	0	C.e./2 D.m./3 A.t./8	H.s./14 M.m./14
pARGs	Ha.V./1	0	0	C.e./1 D.m./1 A.t./1	H.s./1 M.m./1

The number of finished genome sequences for each phylogenetic class is shown on top. Species abbreviations are followed by the number of recognizable respective gene family members. Abbreviations in Tables 2 and 3: Vertebrate: G.g. *Gallus gallus*, H.s. *Homo sapiens*, M.m. *Mus musculus*, Nonvertebrate eucaryotes: A.t. *Arabidopsis thaliana*, C.e. *Caenorhabditis elegans*, D.m. *Drosophila melanogaster*, P.r. *Piris rapae*, T.c. *Tripedalia cystophora*, Archaea: A.f. *Archaeoglobus fulgidus*, M.j. *Methanococcus jannaschii*, Bacteria: A.b. *Azospirillum brasilense*, A.a. *Aquifex aeolicus*, B.c. *Bacillus cereus*, B.h. *Bacillus halodurans*, B.s. *Bacillus subtilis*, B.p. *Bordetella pertussis*, C.b. *Clostridium botulinum*, C.d. *Clostridium difficile*, C.p. *Clostridium perfringens*, D.r. *Deinococcus radiodurans*, E.c. *Escherichia coli*, L.m. *Listeria monocytogenes*, M.l. *Mesorhizobium loti*, P.a. *Pseudomonas aeruginosa*, S.a. *Staphylococcus aureus*, S.c. *Streptomyces coelicolor*, S.p. *Streptococcus pyogenes*, R.r. *Rhodospirillum rubrum*, V.c. *Vibrio cholerae*, V.f. *Vibrio fischeri*, V.p. *Vibrio parahaemolyticus*, Y.e. *Yersinia enterocolitica*, Plasmids: E.c.P. *Escherichia coli* phage; C.b.ph. *Clostridium botulinum* phage; C.d.ph. *Corynebacterium diphtheria* phage; Ch.V. *Paramecium bursaria* *Chlorella* virus, Ci.V. *Chilo iridescent* virus, Ha.V. *Helicoverpa nuclear polyhedrosis* virus.

the respective genes from bacteria to the vertebrate (or pre-vertebrate) lineage enzymes (Andersson et al. 2001; Lander

et al. 2001). It is of interest to note that many bacterial ARTs are encoded by mobile genetic elements, including bacteriophages (ALT, C3 exoenzyme, diphtheria toxin), pathogenicity island (cholera toxin), and plasmid (SpvB), which could facilitate horizontal gene transfer.

Only four open reading frames of unknown function from bacterial genomes showed significant sequence identity to the mART family (Table 2). The likely significance of these matches is underscored by our recent demonstration that one of these, the SpvB virulence factor of *Salmonella*, indeed, is an actin-specific mART (Otto et al. 2000; Tezcan-Merdol et al. 2001). By analogy, the other mART-related proteins encoded by these open reading frames are candidate virulence factors (Pallen et al. 2001).

Note that PSI-BLAST failed to connect two small groups of known bacterial mARTs to the R-S-E family (*Vibrio fischeri* halovibrin alpha and beta, *E. coli* phage modA and modB; Table 2), whereas structure threading programs (Ferstine et al. 1996) reveal that these, indeed, contain an R-S-E motif (Bazan and Koch-Nolte 1997; Wilkens et al. 1997). Evidently the sequences of these mARTs (and the lengths of their connecting loops between conserved  $\beta$ -strands) have diverged too far to be connected with PSI-BLAST. The same holds for the two diphtamide-specific H-Y-E mARTs of *Corynebacterium diphtheria* and *Pseudomonas aeruginosa*, and for the large H-Y-E subgroup of pARTs. Hence, it is possible that other orphan open reading frames in the genome databases encode unidentified ARTs. Indeed, a recent study using PSI-BLASTs to search databases of unfinished prokaryotic genomes uncovered several additional putative bacterial ARTs (Pallen et al. 2001). It is much less likely that family members were missed among orphan open reading frames in the case of ARHs, for which sequence identities between pro- and eucaryotic family members are much higher than for ARTs.

Several organisms evidently encode both ARTs and ARHs, implicating the presence of endogenous ADP-ribosylation cycles as demonstrated in photosynthetic bacteria (Ludden 1994). Others apparently contain only one of these enzymes (Table 3). In the sole presence of ARTs these often function as virulence factors. Conversely, endogenous ARHs might protect against the deleterious effects of pathogen-encoded ART. For example, it is conceivable that the endogenous ARH of *E. coli* serves to protect against phage-encoded mARTs (e.g., mod and ALT).

Last, but not least, the results of this study pave the way for future investigations. *Art* knock-out mice are currently being generated in our laboratories to further elucidate the role of these interesting exoenzymes. Moreover, the recombinant ARTs will facilitate the development of ART inhibitors and of ART-specific antibodies. These hold promise as novel tools for therapeutic interventions.

**Table 4.** ART-specific primers used in this study

Primer	Application	Gene	Location	Nucleotide sequence
M14f	3'RACE	mArt1	exon 4	GAGGACACCTTCTTCGGTATC
T27f	3'RACE	mArt3	exon 9	CAACCCAGATATGGACAATCAGAAGC
T25f	3'RACE	mArt3	exon 11	CAACCTTGACCCTGACAGAATGCC
S02f	3'RACE	mArt4	exon 2	GGCCAGTTCCTCTCTGCCTCCCT
S05f	3'RACE	mArt4	exon 3	GTGGTTATCGTCTGTCTCTTTTGG
N02f	3'RACE	mArt5	exon 4	ACTCTCTGGAGTTATGATCAGACCTG
N03f	3'RACE	mArt5	exon 6	GCTGCAGCTCTCCAGAGCTGGACC
T41r	5'RACE	mArt3	exon 6	ACTCCAAAGCAGGTCTGGATGGTTAGCAC
M33r	5'RACE	mArt1	exon 4	GGCAGGGCCGCTGTCATG
T46r	5'RACE	mArt3	exon 5	CTTCACCTGGAAGATGTCCATTAGAAC
S34r	5'RACE	mArt4	exon 1	CCTCCTGGAAGCCACAGCGCCAT
S35f	5'RACE	mArt4	exon 1	GCATGCARGGGAATGCCAAGGGT
N07r	5'RACE	mArt5	exon 2	CGTAGTTAAGTCGCCAAATCTGTC
N10r	5'RACE	mArt5	exon 3	TGGAGGGGAGTGTGGCTTGG
M18f	MTC	mArt1	exon 1	CAGCTTTGCCCGCCATGGAGAAGGC
M16f	MTC	mArt1	exon 4	CATGACAGCGGCCCTGCC
M90r	MTC	mArt1	exon 6	GCCTGGTACTACCACTCATACC
M15f	MTC	hART1	exon 1	GGACAAGGCCTAGATGAGG
T23f	MTC	mArt3	exon 5	ATGAAGATGGGACATTTTGAAATGGTCAC
T47r	MTC	mArt3	exon 14	TCTGGACTTCCTGTGGGATCCC
S03f	MTC	mArt4	exon 1	GATGGCGCTGTGGCTTCCAGGAGG
S99r	MTC	mArt4	exon 3	AGCAGCTCCTTTAAAAAAGGAGCCAG
L00f	MTC	hART4	exon 1	CCTCCTGCAACGATGAGAATCTGGCTCC
L99r	MTC	hART4	exon 3	GGAGCCACAAGATTTCTTTATACTCTGC
N00f	MTC	mArt5	exon 3	AGGATGATTCTGGAGGATCTGCTGATG
N99r	MTC	mArt5	exon 6	CTGCTTCCTGCAGCCGTTCAAAGCCC
B11f	Zoo-PCR	mArt1	exon 3	CTTTGATGACCAGTACGAGGGCTG
B32r	Zoo-PCR	mArt1	exon 3	CATAGCCTGGGATCAGCACCTCCTC
T21f	Zoo-PCR	mArt3	exon 6	GTGCTAACCATCCAGACCTGCTTTGGAGT
T42r	Zoo-PCR	mArt3	exon 6	CCGAGGAATGCGCACTCGTAGTAGCTGAGGT
L11f	Zoo-PCR	mArt4	exon 2	TCTTTTGATGATCAGTACCAAGGCTG
L42r	Zoo-PCR	mArt4	exon 2	AACTTTAAACAGCTCATAGGGAGG
N11f	Zoo-PCR	mArt5	exon 4	GATACCTTTGATGATGCCTATGTGGGCTG
N41r	Zoo-PCR	mArt5	exon 4	GACAACGCCTGGATAGGAGCCCCAAAACA
TT01f	chr.mapping	mArt3	intron	CACGCACTCACATACACAATGTGCC
TT31r	chr.mapping	mArt3	intron	TGATATGATGCCTTCTGGCCCTACC
S21f	chr.mapping	mArt4	intron	CTCCTGAGACAGGGACAGAGAATCAAG
S51r	chr.mapping	mArt4	intron	TTTCTAGGTACTAGGGGGTTCAGACTG

Data deposition requirements: The sequences described here have been deposited in the EMBL database (see Table 1 for accession numbers).

## Materials and methods

### Isolation and sequencing of cDNA and genomic DNA

ART-specific primers used in this study are listed in Table 4 ("f" and "r" in primer names indicate forward or reverse orientation of the primer). Human and mouse cDNAs were subjected to 5' and 3' rapid amplification of cDNA ends (RACE) according to the manufacturer's (Clontech) protocol. Genomic DNAs were prepared as described previously (Koch et al. 1990; Koch-Nolte et al. 1993, 1997). IMAGE consortium ESTs and P1, PAC, and BAC genomic DNA clones were obtained from Genome Systems, and the Resource Center of the German Genome Project (rzpd). Genomic DNA libraries were screened by PCR with ART-specific primers or by hybridization with ART-specific probes. Exon-containing fragments were generated by restriction digestion or PCR amplification, subcloned into plasmids (pBluescript, Stratagene, and

pCR2.1, Invitrogen) and sequenced. Sequences obtained from PCR products were confirmed by sequencing clones obtained from two separate PCR reactions.

### Cross-species "Zoo" PCR

Primers for "Zoo" PCR were designed from regions where known ARTs showed strong sequence similarity, for example, primers ended in codons for a conserved cysteine or the catalytic glutamic acid residue. PCR reactions were carried out with genomic DNAs (100–500 ng) from different mammalian species using "hot start" and "touch-down" techniques with Amplitaq Gold polymerase (Stratagene). The initial denaturation was for 8 min at 96°C, followed by 33 cycles for 20 sec at 95°C. The annealing temperature was decreased successively in 5° intervals from 70 to 35°C in the first eight cycles followed by 25 cycles at 65°C. Annealings were

performed for 20 sec, extensions for 60 sec (at 72°C), with a final extension of 8 min.

### *Chromosomal mapping, Southern and Northern blot analyses*

Map positions for human ART genes were determined by PCR screening of genomic DNAs from rodent/human somatic cell hybrids as described previously (Koch-Nolte et al. 1993, 1996a). Map positions were confirmed by BLASTn analyses of the recently published human genome sequence (Lander et al. 2001). Mouse *Art* genes were mapped by PCR screening (*Art3*, *Art4*) or by Southern blot analyses (*Art1*, *Art2a*, *Art2b*, *Art5*) of a panel of 94 genomic DNAs from the (C57BL/6JEi × SPRET/Ei) × SPRET/Ei (BSS) backcross panel available from The Jackson Laboratory Mapping Panel Resource (Rowe et al. 1994). PCR primers flanking informative polymorphic microsatellite repeats in *Art3* and *Art4* in both cases yielded ~200 bp C57BL/6J products versus slightly smaller SPRET/Ei products. Informative restriction fragment length variants (RFLVs) used for mapping the other *Art* genes were: *Bam*HI RFLVs for *Art1*, *Art2a*, and *Art3* (6.7, 3.7, and 3.0 kb SPRET/Ei fragments, respectively, versus slight smaller fragments in C57BL/6J), and a *Taq*I RFLV for *Art5* (C57BL/6J ~1.7 kb, SPRET/Ei ~2.0 kb). Southern and Northern blot analyses were performed as described previously (Koch et al. 1990; Koch-Nolte et al. 1997; Braren et al. 1998).

### *Expression of recombinant ART proteins and enzyme assays*

Baculovirus constructs for producing soluble ARTs in which the hydrophobic C-terminal GPI-anchor signal sequence were replaced by tandem His6x and FLAG epitope tags were prepared as described previously (Koch-Nolte et al. 1996b). Recombinant ARTs were purified from insect cell supernatants by affinity chromatography on Talon-columns (Clontech) or Sepharose-immobilized anti-FLAG M2 monoclonal antibody (Sigma), and were incubated in 50 µL enzyme buffer (20 mM Tris pH 8.0, 1 mM ADP-ribose, 5 mM DTT, 2 mM agmatine, 5 µM 32P-NAD+, 0.5 µCi, Amersham-Pharmacia) for 60 min at 37°C. Proteins were analyzed by SDS-PAGE and Western b/F11i73.7(a;.8(b/F1-355.1(solb/F1reac38.1(in-) Trestri4wer/6J)-458(prodwer/6-306dwer7)-3itri4wer/6lay.2(buwe

- Haag, F., Andresen, V., Karsten, S., Koch-Nolte, F., and Thiele, H. 1995. Both allelic forms of the rat T cell differentiation marker RT6 display nicotinamide adenine dinucleotide (NAD)-glycohydrolase activity, yet only RT6.2 is capable of automodification upon incubation with NAD. *Eur. J. Immunol.* **25**: 2355–2361.
- Haag, F. and Koch-Nolte, F. 1997. *ADP-ribosylation in animal tissues: Structure, function and biology of mono(ADP-ribosyl)transferases and related enzymes*. Plenum Press, New York.
- Haag, F., Koch-Nolte, F., Kühn, M., Lorenzen, S., and Thiele, H.G. 1994. Premature stop codons inactivate the RT6 genes of the human and chimpanzee species. *J. Mol. Biol.* **243**: 537–546.
- Haag, F., Kühlenbäumer, G., Koch-Nolte, F., Wingender, E., and Thiele, H.G. 1996. Structure of the gene encoding the rat T cell ecto-ADP-ribosyltransferase RT6. *J. Immunol.* **157**: 2022–2030.
- Han, S., Arvai, A.S., Clancy, S.B., and Tainer, J.A. 2001. Crystal structure and novel recognition motif of rho ADP-ribosylating C3 exoenzyme from *Clostridium botulinum*: Structural insights for recognition specificity and catalysis. *J. Mol. Biol.* **305**: 95–107.
- Han, S., Craig, J.A., Putnam, C.D., Carozzi, N.B., and Tainer, J.A. 1999. Evolution and mechanism from structures of an ADP-ribosylating toxin and NAD complex. *Nat. Struct. Biol.* **6**: 932–936.
- Jacobson, M.K. and Jacobson, E.L. 1989. *ADP-ribose transfer reactions: Mechanisms and biological significance*. Springer Verlag, New York.
- Koch, F., Haag, F., Kashan, A., and Thiele, H.G. 1990. Primary structure of rat RT6.2, a nonglycosylated phosphatidylinositol-linked surface marker of postthymic T cells. *Proc. Natl. Acad. Sci.* **87**: 964–967.
- Koch-Nolte, F., Haag, F., Braren, R., Kuhl, M., Hoovers, J., Balasubramanian, S., Bazan, F., and Thiele, H.G. 1997. Two novel human members of an emerging mammalian gene family related to mono-ADP-ribosylating bacterial toxins. *Genomics* **39**: 370–376.
- Koch-Nolte, F., Haag, F., Kühn, M., van Heyningen, V., Hoovers, J., Grzeschik, K. H., Singh, S., and Thiele, H.G. 1993. Assignment of the human RT6 gene to 11q13 by PCR screening of somatic cell hybrids and *in situ* hybridization. *Genomics* **18**: 404–406.
- Koch-Nolte, F., Kühn, M., Haag, F., Cetkovic-Cvrlje, M., Leiter, E.H., and Thiele, H.G. 1996a. Assignment of the human and mouse genes for muscle ecto mono (ADPribosyl)transferase to a conserved linkage group on human chromosome 11p15 and mouse chromosome 7. *Genomics* **36**: 215–216.
- Koch-Nolte, F., Petersen, D., Balasubramanian, S., Haag, F., Kahlke, D., Willer, T., Kastelein, R., Bazan, F., and Thiele, H.G. 1996b. Mouse T cell membrane proteins Rt6-1 and Rt6-2 are arginine/protein mono(ADPribosyl)transferases and share secondary structure motifs with ADP-ribosylating bacterial toxins. *J. Biol. Chem.* **271**: 7686–7693.
- Lander, E.S., Linton, L.M., et al. 2001. Initial sequencing and analysis of the human genome. *Nature* **409**: 860–921.
- Ludden, P.W. 1994. Reversible ADP-ribosylation as a mechanism of enzyme regulation in prokaryotes. *Mol. Cell. Biochem.* **138**: 123–129.
- Marra, M.A., Hillier, L., and Waterston, R.H. 1998. Expressed sequence tags—ESTablishing bridges between genomes. *Trends. Genet.* **14**: 4–7.
- Moss, J., Stanley, S.J., Nightingale, M.S., Murtagh, J.J., Monaco, L., Mishima, K., Chen, H.C., Williamson, K.C., and Tsai, S.C. 1992. Molecular and immunological characterization of ADP-ribosylarginine hydrolases. *J. Biol. Chem.* **267**: 10481–10488.
- Okazaki, I.J. and Moss, J. 1998. Glycosylphosphatidylinositol-anchored and secretory isoforms of mono-ADP-ribosyltransferases. *J. Biol. Chem.* **273**: 23617–23620.
- Okazaki, I.J., Kim, H.J., and Moss, J. 1996. Cloning and characterization of a novel membrane-associated lymphocyte NAD:arginine ADP-ribosyltransferase. *J. Biol. Chem.* **271**: 22052–22057.
- Okazaki, I.J., Zolkiewska, A., Nightingale, M.S., and Moss, J. 1994. Immunological and structural conservation of mammalian skeletal muscle glycosylphosphatidylinositol-linked ADP-ribosyltransferases. *Biochemistry* **33**: 12828–12836.
- Otto, H., Tezcan-Merdol, D., Girisch, R., Haag, F., Rhen, M., and Koch-Nolte, F. 2000. The spvB gene-product of the *Salmonella enterica* virulence plasmid is a mono(ADP-ribosyl)transferase. *Mol. Microbiol.* **37**: 1106–1115.
- Pallen, M.J., Lam, A.C., Loman, N.J., and McBride, A. 2001. An abundance of bacterial ADP-ribosyltransferases—Implications for the origin of exotoxins and their human homologues. *Trends Microbiol.* **9**: 302–307.
- Piatigorsky, J. 1998. Multifunctional lens crystallins and corneal enzymes. More than meets the eye. *Ann. NY Acad. Sci.* **842**: 7–15.
- Rappuoli, R. and Montecucco, C. 1997. *Guidebook to protein toxins and their use in cell biology*. Oxford University Press, Oxford.
- Rost, B. and Sander, C. 1993. Improved prediction of protein secondary structure by use of sequence profiles and neural networks. *Proc. Natl. Acad. Sci.* **90**: 7558–7562.
- Rowe, L., Nadeau, J., Turner, R., Frankel, W., Letts, V., Eppig, J., Ko, M., Thurston, S., and Birkenmeier, E. 1994. Maps from two interspecific backcross DNA panels as a community mapping resource. *Mammal. Genome* **5**: 253–274.
- Ruf, A., Menissier de Murcia, J., De Murcia, G., and Schulz, G.E. 1996. Structure of the catalytic fragment of poly(ADP-ribose)polymerase from chicken. *Proc. Natl. Acad. Sci.* **93**: 7481–7485.
- Smith, S. 2001. The world according to PARP. *Trends Biochem. Sci.* **26**: 174–179.
- Tezcan-Merdol, D., Nyman, T., Lindberg, U., Haag, F., Koch-Nolte, F., and Rhen, M. 2001. Actin is ADP-ribosylated by the *Salmonella enterica* virulence-associated protein SpvB. *Mol. Microbiol.* **39**: 606–619.
- Tschopp, J., Irmiler, M., and Thome, M. 1998. Inhibition of fas death signals by FLIPs. *Curr. Opin. Immunol.* **10**: 552–558.
- Wilde, C., Chhatwal, G.S., Schmalzing, G., Aktories, K., and Just, I. 2001. A novel C3-like ADP-ribosyltransferase from *Staphylococcus aureus* modifying RhoE and Rnd3. *J. Biol. Chem.* **276**: 9537–9542.
- Wilkins, K., Tiemann, B., Bazan, F., and Ruger, W. 1997. ADP-ribosylation and early transcription regulation by bacteriophage T4. *Adv. Exp. Med. Biol.* **419**: 71–82.
- Wilson, B.A. and Collier, R.J. 1992. Diphtheria toxin and *Pseudomonas aeruginosa* exotoxin A: Active-site structure and enzymic mechanism. *Curr. Top. Microbiol. Immunol.* **175**: 27–41.